# Charge Localization Dynamics Induced by Oxygen Vacancies on the $TiO_2$(110) Surface

Piotr M. Kowalski,* Matteo Farnesi Camellone, Nisanth N. Nair,† Bernd Meyer,‡ and Dominik Marx

*Lehrstuhl für Theoretische Chemie, Ruhr–Universität Bochum, 44780 Bochum, Germany*

(Received 25 June 2010; published 30 September 2010)

The dynamics of an $F$ center created by an oxygen vacancy on the $TiO_2$(110) rutile surface has been investigated using *ab initio* molecular dynamics. These simulations uncover a truly complex, time-dependent behavior of fluctuating electron localization topologies in the vicinity of the oxygen vacancy. Although the two excess electrons are found to populate preferentially the second subsurface layer, they occasionally visit surface sites and also the third subsurface layer. This dynamical behavior of the excess charge explains hitherto conflicting interpretations of both theoretical findings and experimental data.

DOI: 10.1103/PhysRevLett.105.146405 PACS numbers: 71.15.Pd, 73.20.At, 73.20.Jc, 82.65.+r

Titanium dioxide ($TiO_2$) is one of the most thoroughly investigated metal oxides, due to its broad range of uses in several key technologies including heterogeneous catalysis, pigment materials, photocatalysis, and energy production, to name but a few [1–3]. It is well known that bulk and surface defects govern the properties of titania, and are thus of fundamental importance in virtually all its applications [4–6]. The most common point defects on the $TiO_2$(110) rutile surface are oxygen vacancies ($O_v$) in the twofold coordinated O rows and Ti interstitials [7,8]. In particular, removal of an O atom gives rise to two excess electrons and the appearance of new electronic states in the band gap at about 0.7–0.9 eV below the conduction band edge creating an $F$ center [9–11]. Although the two excess electrons can in principle be localized on any Ti atom, they are believed to preferentially occupy specific Ti-3$d$ orbitals, thus formally creating $Ti^{3+}$ sites [10,12]. In stark contrast, recent experiments [13] suggest a qualitatively different viewpoint: charge localization is found to be more disperse, with the excess electrons being shared by several surface and subsurface Ti ions. Furthermore, STM and STS experiments have revealed charge delocalization involving more than ten Ti sites [14].

Unfortunately, different computational methods yield conflicting results [11]. Local or semilocal density functionals (LDA/GGA) predict a rather delocalized defect level for O vacancies on $TiO_2$(110) with an energy right at the bottom of the conduction band [11]. However, it is well known that such functionals bias against localization on strongly correlated $d$ states, and hence alternative methodologies are welcome. Recent studies of defective $TiO_2$ surfaces [15–21] have focused on "pragmatic and practical" correction schemes using hybrid functionals or a Hubbard correction. Although both schemes yield the expected gap states, they each predict vastly different localization topologies of the excess charge.

Using B3LYP on a $c(4 \times 2)$ slab with an O vacancy, the defect charge is found to be localized on $d$ orbitals of two surface Ti atoms [15]. In particular, one unpaired electron is found on the undercoordinated Ti(11) site, while the other moves to an adjacent fivefold coordinated $Ti_{5c}$ atom, such as Ti(7); see Fig. 1 for our site labeling scheme. By contrast, LDA/GGA + $U$ studies [16–21] on the reduced $TiO_2$(110) surface have reported charge localization on different surface and/or subsurface sites. For instance, a combination of surface and subsurface localization immediately beneath the defect on Ti(11) and Ti(27) (see Fig. 1) has been found [16]. However, the results are reported to be strongly dependent on the supercell size. Using a $(2 \times 1)$ cell, the electrons are found at Ti(7) and Ti(23), while using a $(4 \times 1)$ cell complete subsurface localization is observed [21] at Ti(23) and Ti(39). On the other hand, a $(4 \times 2)$ cell yields localization of the electrons on Ti(11) and Ti(12) when using $U \geq 4.2$ eV, whereas smaller values of $U$ lead instead to delocalization [19]. Interestingly, some recent GGA + $U$ studies [22,23] which focussed on

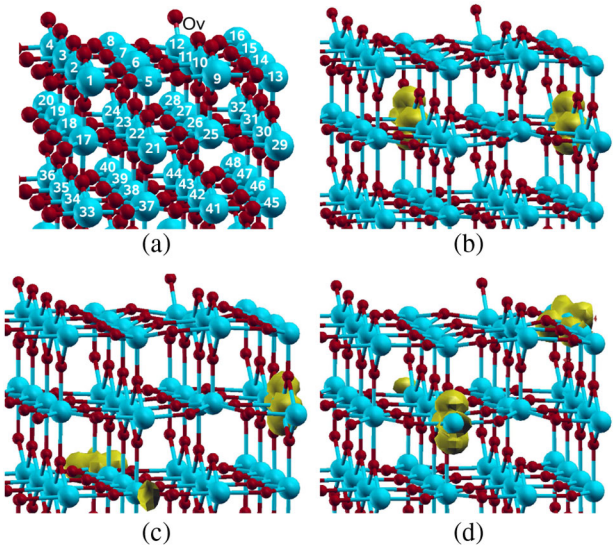


FIG. 1 (color online). (a) Ball and stick model of the defective $TiO_2$(110) surface. Red (dark gray) and blue (light gray) spheres are O and Ti atoms, respectively. Panels (b), (c), and (d) depict the spin density (at 0.005 $e/Å^3$) of three configurations from Table I with different charge localization topologies.

 

the intrinsic electron transport in titania provide useful hints: Electron hopping in defect-free $TiO_2$ bulk [22] is described by a polaron localized at a $Ti^{3+}$ site, which can hop to an adjacent $Ti^{4+}$ with activation energies of only $\approx 0.1$ eV. Furthermore, static calculations of ideal $TiO_2(110)$ surfaces with a single excess electron suggest that the most favorable trapping sites are subsurface ions that lie below rows of $Ti_{5c}$ atoms on the surface [23].

In summary, the existing results of electronic structure calculations which suggest highly localized excess electrons at very specific Ti sites are at odds with the current experimental picture of a more ''fuzzy'' scenario involving many sites and delocalized excess charge. However, low activation energies (of the order of 0.1 eV) and the multitude of topologies for the localization of excess charge that have been previously revealed suggest that the energy landscape might be relatively flat and thus prone to thermal fluctuations which could affect localization scenarios in a dynamical sense.

In this Letter, we describe extensive GGA + *U ab initio* molecular dynamics (AIMD) simulations [24] of the excess charge (de-)localization dynamics as induced by temperature. We find that the defect charge created by an O vacancy on $TiO_2(110)$ is dynamically shared by several subsurface and surface Ti sites, with a dominant contribution from particular second-layer subsurface sites which do not belong to $O_b$ rows. Thermal fluctuations of the titania lattice allow the excess charge to probe—and thus to populate—various local (electronic structure) minima of similar energy but vastly different localization topologies. Our findings demonstrate the need to go beyond static optimization in order to uncover the dynamical nature of the phenomenon. These results strongly support the proposal of a delocalized nature of the excess charge for such defects, and in addition, they also reconcile the hitherto contradictory viewpoints from different static electronic structure calculations.

The reduced $TiO_2(110)$ surfaces have been modeled by four O-$Ti_2O_2$-O trilayer ($4 \times 2$) supercell slabs, separated by more than 10 Å (see Fig. 1). The bottom of the slab was passivated with pseudohydrogen atoms of nuclear charge $+4/3$ and $+2/3$ in order to achieve well converged results, which is our ''standard setup'' [25]. All calculations have been performed using spin-polarized GGA + *U*, Perdew-Burke-Ernzerhof exchange-correlation functional (PBE) [26], and ultrasoft pseudopotentials [27]. Extending our previous work [25], we have implemented GGA + *U* into CPMD [28] using the self-consistent linear response approach [29,30] to compute the Hubbard parameter, yielding $U = 4.2$ eV for our setup; as usual the localization details will depend on the particular value of *U*, but the qualitative features reported in this Letter were checked to be stable upon reasonable variation. The occupations of the *d* orbitals are calculated using atomiclike wave function projectors. The lowest trilayer atoms are constrained to their equilibrium positions, while all other atoms are free to move. The AIMD simulations [24] were on the order of 10 ps in length, and used the Car-Parrinello propagation technique [31] with a fictitious electron mass of 700 a.u. and a time step of 0.145 fs.

In order to reveal the nature and distribution of the defect charge, we performed the PBE + *U* simulations at various temperatures, ranging from 700 to 1000 K. This is well below the melting point of almost 2000 K, but sufficiently far above the ambient temperature that the phonon dynamics is accelerated and thus the sampling of the potential energy surface is enhanced on the picosecond AIMD time scale. Two complementary scenarios, characterized by different defect charge localization topologies, were employed in order to provide two distinct sets of initial conditions. One scenario represents a case where the two excess electrons are trapped at two second layer sites, Ti(24) and Ti(30), under $Ti_{5c}$ rows. The second scenario corresponds to localization on an undercoordinated site in the first layer, Ti(11), and on Ti(29) in the second layer under a $Ti_{5c}$ row. In both cases the paramagnetic triplet state is preferred and the structure with the defect charge localized on the second layer is roughly 0.6 eV more stable (see Table I).

After equilibrating both setups at 300 K for about 2 ps each, the systems were heated to their respective simulation temperatures. The charge localization dynamics was monitored by computing, as a function of time, the occupation matrix of each Ti $d$-$\alpha$ and $d$-$\beta$ spin orbital along the trajectories. We will first consider the effect induced by thermal fluctuations on the setup with all excess

TABLE I. Relative energies (in eV) and Ti(11)-O bond lengths (in Å) of reduced $TiO_2(110)$ with different localization of the $O_v$-induced excess charge. The last three columns show on which layer(s) the two excess electrons are localized. Bold labels refer to the configurations in Fig. 1.

| $Ti^{3+}$ | $Ti^{3+}$ | $\Delta E$ | Ti(11)-O | 1st-layer | 2nd-layer | 3rd-layer |
|---|---|---|---|---|---|---|
| Ti(6) | Ti(32) | 0.23 | 1.87 | 1*e* | 1*e* | 0*e* |
| **Ti(15)** | **Ti(21)** | 0.28 | 1.87 | 1*e* | 1*e* | 0*e* |
| Ti(11) | Ti(29) | 0.77 | 1.92 | 1*e* | 1*e* | 0*e* |
| **Ti(24)** | **Ti(31)** | 0.00 | 1.87 | 0*e* | 2*e* | 0*e* |
| Ti(22) | Ti(29) | 0.04 | 1.87 | 0*e* | 2*e* | 0*e* |
| Ti(24) | Ti(30) | 0.16 | 1.86 | 0*e* | 2*e* | 0*e* |
| Ti(27) | Ti(29) | 0.22 | 1.86 | 0*e* | 2*e* | 0*e* |
| **Ti(30)** | **Ti(40)** | 0.36 | 1.87 | 0*e* | 1*e* | 1*e* |

charge initially localized in the second layer. As demonstrated by Fig. 2(a), the defect charge transfers from sites Ti(24) and Ti(31) to Ti(21) and Ti(32) in less than 0.5 ps; we note in passing that a qualitatively similar scenario is observed using a smaller $(2 \times 1)$ cell. Approximately 30 such charge migration events were observed during the 6 ps simulation, although only a few of them involve charge leaving the second subsurface layer and moving to the first or third layer. This implies that the defect charge spends most of the time at second-layer Ti ions, but translocates very rapidly from a given Ti site to an adjacent one within the same subsurface row. We observed no charge transfer to Ti sites belonging to adjacent rows. Other interesting electronic topologies explored by the dynamics are cases in which the two excess electrons are localized simultaneously on second- and first-layer sites, for example, on Ti(32) and Ti(6) or on Ti(21) and Ti(15). Furthermore, a configuration has been sampled where the excess charge is shared between the second and third layer involving Ti(30) and Ti(40). The average lifetime for a specific charge-localized topology is roughly 0.3 ps at 1000 K, which underscores the pronounced dynamical nature of the phenomenon. At 700 K, this time scale increases to about 0.4 ps, from which naive Arrhenius extrapolation yields a formal activation energy of approximately 0.07 eV and lifetimes of the order of ps and ns to $\mu$s at ambient and liquid nitrogen temperatures, respectively. This implies that dynamical averaging up to quenched disorder at liquid helium conditions might be operational in surface science experiments.

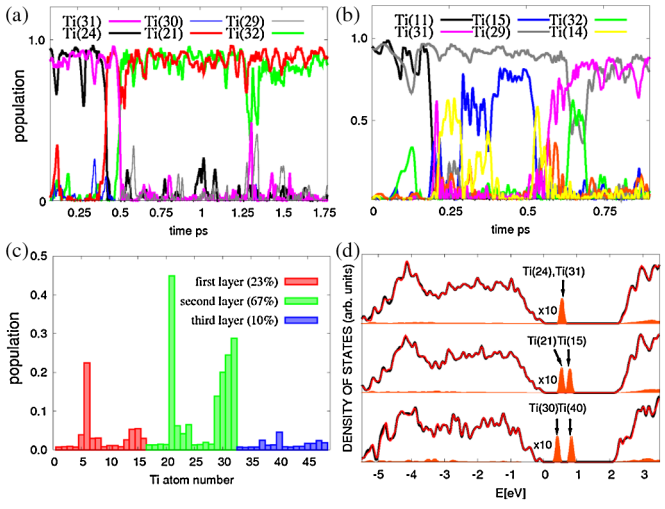


FIG. 2 (color online). (a) Dynamics of the fractional occupation of particular Ti $d$ orbitals during a time fragment of the PBE + $U$ simulation carried out at 1000 K; at $t = 0$ the charge is localized in the second subsurface layer at Ti(24) and Ti(31); populations of about 1 and 0 correspond to $Ti^{3+}$ and $Ti^{4+}$ charge states, respectively. (b) Same as (a) but the charge is initially localized in the first layer at Ti(11) and subsurface at Ti(29) at 700 K. (c) Distribution function of the average population of all available Ti sites by the two excess electrons obtained from the full simulation underlying (a); inset provides layer-averaged populations. (d) Electronic density of states ($\alpha$ ($\beta$) spins: red (black) lines) of the three structures from Fig. 1; peaks in the band gap correspond to reduced Ti sites; the top of the valence band is set to 0 eV, and the red area filling the gap states (scaled by 10 to enhance visibility) stems from $Ti^{3+}$ sites as labeled.

Next we consider the complementary scenario where the defect charge is localized initially in both the first and second layers at Ti(11) and Ti(29) [see Fig. 2(b)]. After only 0.1–0.2 ps, the charge at Ti(11) transfers from the $O_b$ surface row to the adjacent surface row of $Ti_{5c}$ atoms where it is delocalized over two nearest-neighbor sites Ti(14) and Ti(15). It remains shared between these two sites for about 0.5 ps before it jumps to the nearest-neighbor second-layer atom, Ti(31). Here, charge transfer between the first and second layers is found to be mediated by a charge delocalization process involving first-layer Ti sites in the $Ti_{5c}$ row. Once the charge reaches the second layer, during the next $\approx 4$ ps it visits the same Ti sites as it had earlier explored. In one of these events a flipping of one of the two unpaired electrons between an $\alpha$- and $\beta$-$d$ orbital occurs along the trajectory.

The dynamical behavior can be cast into distribution functions using localization histograms, which is illustrated in Fig. 2(c) for the dynamics in (a). In both setups the excess charge is found to be extremely mobile and to eventually visit all available Ti sites, although it displays a strong preference for populating sites in the second subsurface layer under the $Ti_{5c}$ rows (roughly 70%). This is followed by population of surface states ($\approx 20\%$), and localization in the third subsurface layer ($\approx 10\%$). We note that in all observed charge transfer events there was always a mediating nearest-neighbor Ti site transiently involved in the process. This dynamical scenario is in substantial agreement with the viewpoint suggested based on recent experiments [13,14].

In order to assess the energetics of the various localization topologies, we have characterized representative structures in detail. Six additional excess charge topologies were obtained by quenching a large set of sampled configurations to $T = 0$ K using Car-Parrinello annealing [24] followed by standard optimization (see Table I). Localization of one excess electron at Ti(11) induces a significant elongation of the $Ti^{3+}$(11)-O distance (see Table I), which is as expected [15,18,19]. The relative energies confirm that the most stable sites for charge localization are those where both electrons are in the second subsurface layer under $Ti_{5c}$ rows—in line with earlier findings [21] and consistent with our localization histograms. About 0.2–0.3 eV higher in energy are the topologies where the excess charge is shared between surface $Ti_{5c}$ atoms and second subsurface layer sites below $Ti_{5c}$ rows. Topologies resulting in excess charge localization on both second and third subsurface layer sites under $Ti_{5c}$ are less stable by about 0.3–0.4 eV. In the least stable configuration, (by 0.7–0.8 eV) one electron is at an undercoordinated surface site, Ti(11) at the $O_b$ vacancy, whereas the other electron has transferred to the second subsurface layer under a $Ti_{5c}$ row at Ti(29). In one case,

starting from a configuration in which the charge is delocalized over two surface atoms, Ti(14) and Ti(15), and one second-layer site, Ti(29), we end up with a solution in which one electron is trapped at Ti(29) under the $Ti_{5c}$ row and the other electron is localized on the Ti site directly below the $O_b$ vacancy. This configuration, which has also been recently reported [16], is found to be 0.22 eV higher in energy than our lowest energy configuration. The concomitant static distortions obtained from the nearest-neighbor $Ti^{3+}$-O distances of the optimized structures (b)–(d) in Fig. 1 relative to the nonrelaxed reference (a) are typically 0.05–0.1 Å. However, already at 300 K the thermal fluctuations are found to override these static distortions by inducing larger root-mean-square deviations of the same relative distances.

Combining our static and dynamic calculations demonstrates that the excess charge dynamics is intimately tied to the existence of many close-lying minima on the potential energy surface which can be populated at finite temperatures [12]. Charge localization patterns from static optimizations therefore depend heavily on the initial configuration due to trapping in local energy minima. This might contribute to the variety of differing results reported in the literature. In this situation, AIMD helps greatly by not only providing a dynamic perspective, but also by being able to explore vastly different localization topologies.

Finally, the total and projected electronic density of states of the distinctly different charge localization scenarios are analyzed in Fig. 2(d). In all cases, the O vacancy leads to the appearance of distinct, filled states in the $TiO_2$(110) band gap, whose projection onto two specific Ti sites—although they are different for each of the three scenarios—fully accounts for the entire peak integral area. Together with the almost instantaneous changes in localization patterns embodied in Figs. 2(a) and 2(b), this indicates that the two excess electrons are essentially always trapped at two well-identified, specific Ti sites. These sites, however, are not unique for a given defect, but rather they interchange dynamically.

In conclusion, finite temperature PBE + $U$ simulations paint a complex picture of the dynamics of electrons in defects at the reduced titania $TiO_2$(110) surface. The excess charge, being trapped at specific Ti sites, migrates easily by phonon-assisted (thermally activated) hopping to other Ti sites, thus exploring significantly different electronic structure topologies. Because of averaging effects, this leads to an ''effective delocalization,'' which is preferentially found on second-layer subsurface Ti atoms underneath $Ti_{5c}$ rows. Although much less frequently, excess charge also ''visits'' first-layer and third-layer subsurface sites. We expect that this defect-induced complex charge (de-)localization dynamics scenario is not only fundamental to titania, but of broad significance to oxide materials in general.

This work has been supported by the German Research Foundation (DFG) via SFB 558, by RD IFSC, and by FCI. Computational resources were provided by Bovilab at RUB (Bochum) as well as RV-NRW.

*Present address: Helmholtz Centre Potsdam, Telegrafenberg, 14473 Potsdam, Germany.
†Present address: Department of Chemistry, Indian Institute of Technology Kanpur, Kanpur 208016, India.
‡Present address: Interdisziplinäres Zentrum für Molekulare Materialien (ICMM) and Computer-Chemie-Centrum (CCC), Universität Erlangen-Nürnberg, 91052 Erlangen, Germany.

[1] B. O'Regan and M. Grätzel, Nature (London) **353**, 737 (1991).
[2] D. Matthey *et al.*, Science **315**, 1692 (2007).
[3] H. Imagawa *et al.*, J. Catal. **251**, 315 (2007).
[4] R. A. Bennett, Phys. Chem. Comm. **3**, 9 (2000).
[5] C. L. Pang, R. Lindsay, and G. Thornton, Chem. Soc. Rev. **37**, 2328 (2008).
[6] A. J. Limb, O. Bikondoa, C. A.Muryn, and G. Thornton, Angew. Chem., Int. Ed. **46**, 549 (2007).
[7] C. M. Yim, C. L. Pang, and G. Thornton, Phys. Rev. Lett. **104**, 036806 (2010).
[8] S. Wendt *et al.*, Science **320**, 1755 (2008).
[9] V. E. Henrich, G. Dresselhaus, and H. J. Zeiger, Phys. Rev. Lett. **36**, 1335 (1976).
[10] U. Diebold, Surf. Sci. Rep. **48**, 53 (2003).
[11] M. V. Ganduglia-Pirovano, A. Hofmann, and J. Sauer, Surf. Sci. Rep. **62**, 219 (2007).
[12] C. Di Valentin, G. Pacchioni, and A. Selloni, J. Phys. Chem. C **113**, 20 543 (2009).
[13] P. Krüger *et al.*, Phys. Rev. Lett. **100**, 055501 (2008).
[14] T. Minato *et al.*, J. Chem. Phys. **130**, 124502 (2009).
[15] C. Di Valentin, G. Pacchioni, and A. Selloni, Phys. Rev. Lett. **97**, 166803 (2006).
[16] A. C. Papageorgious *et al.*, Proc. Natl. Acad. Sci. U.S.A. **107**, 2391 (2010).
[17] E. Finazzi, C. Di Valentin, G. Pacchioni, and A. Selloni, J. Chem. Phys. **129**, 154113 (2008).
[18] B. J. Morgan and G. W. Watson, J. Phys. Chem. C **113**, 7322 (2009).
[19] B. J. Morgan and G. W. Watson, Surf. Sci. **601**, 5034 (2007).
[20] F. Filippone, G. Mattioli, P. Alippi, and A. Amore Bonapasta, Phys. Rev. B **80**, 245203 (2009).
[21] C. J. Calzado, N. C. Hernández, and J. F. Sanz, Phys. Rev. B **77**, 045118 (2008).
[22] N. A. Deskins and M. Dupuis, Phys. Rev. B **75**, 195212 (2007).
[23] N. A. Deskins, R. Rousseau, and M. Dupuis, J. Phys. Chem. C **113**, 14 583 (2009).
[24] D. Marx and J. Hutter, *Ab Initio Molecular Dynamics: Basic Theory and Advanced Methods* (Cambridge University Press, Cambridge 2009).
[25] P. M. Kowalski, B. Meyer, and D. Marx, Phys. Rev. B **79**, 115410 (2009).
[26] J. P. Perdew, K. Burke, and M. Ernzerhof, Phys. Rev. Lett. **77**, 3865 (1996); **78**, 1396(E) (1997).
[27] D. Vanderbilt, Phys. Rev. B **41**, 7892 (1990).
[28] J. Hutter *et al.*, computer code CPMD, www.cpmd.org.
[29] M. Cococcioni and S. de Gironcoli, Phys. Rev. B **71**, 035105 (2005).
[30] H. J. Kulik, M. Cococcioni, D. A.Scherlis, and N. Marzari, Phys. Rev. Lett. **97**, 103001 (2006).
[31] R. Car and M. Parrinello, Phys. Rev. Lett. **55**, 2471 (1985).